The ubiquitous microtubule-associated protein 4 (MAP4) controls organelle distribution by regulating the activity of the kinesin motor

Ibtissem Nabti[a], Babu J. N. Reddy[b], Rachid Rezgui[c], Wenqi Wang[b], Steven P. Gross[b], and George T. Shubeita[a,1]

Regulation of organelle transport by molecular motors along the cytoskeletal microtubules is central to maintaining cellular functions. Here, we show that the ubiquitous tau-related microtubule-associated protein 4 (MAP4) can bias the bidirectional transport of organelles toward the microtubule minus-ends. This is concurrent with MAP4 phosphorylation, mediated by the kinase GSK3β. We demonstrate that MAP4 achieves this bias by tethering the cargo to the microtubules, allowing it to impair the force generation of the plus-end motor kinesin-1. Consistent with this mechanism, MAP4 physically interacts with dynein and dynactin and, when phosphorylated, associates with the cargo–motor complex through its projection domain. Its phosphorylation coincides with the perinuclear accumulation of organelles, a phenotype that is rescued by abolishing the cargo–microtubule MAP4 tether or by the pharmacological inhibition of dynein, confirming the ability of kinesin to inch along, albeit inefficiently, in the presence of phosphorylated MAP4. These findings have broad biological significance because of the ubiquity of MAP4 and the involvement of GSK3β in multiple diseases, more specifically in cancer, where the MAP4-dependent redistribution of organelles may be prevalent in cancer cells, as we demonstrate here for mitochondria in lung carcinoma epithelial cells.

MAP4 | microtubule-associated protein 4 | GSK3 | kinesin | microtubule-based transport

The internal organization of the cell is indispensable for many of its functions. Essential to this organization is the system of intracellular transport through which different cargoes are actively transported by molecular motors along the cell cytoskeletal filaments to their appropriate destination. Much of the long-range active transport in cells depends on the cytoplasmic dynein and kinesin families of motor proteins, which move toward the minus-end (toward the cell center) and plus-end of microtubules (toward the cell periphery), respectively (1, 2). Cargoes hauled by motors include RNA granules, chromosomes, and different membrane-bound organelles, highlighting the importance of this transport system for various biological processes. The diversity of cargoes also underscores the complexity of transport since a handful of motor types need to transport a wide range of cargoes to various places at the same time. Therefore, maintaining the proper distribution of cargoes by tightly regulating the transport machinery is indispensable, given that any defects are often associated with serious developmental and neurodegenerative diseases (1, 3).

Within the cell, many cargoes move bidirectionally, although the motors that transport them mostly move unidirectionally (4–7). To maintain robust delivery or distribution of cargo, bidirectional transport needs to be tightly regulated. Various mechanisms of regulation have been described, implicating specific motor cofactors, adaptors, or regulators (4, 7–10). However, the molecular mechanisms of motor regulation are rarely understood, although examples whereby regulation was shown to target aspects of motor stepping, force sensitivity, and detachment characteristics have been reported (11–14). The increasing understanding of the function of isolated motors and the stark differences that have emerged in the details of opposite-polarity motor stepping and force sensitivity (6, 15, 16) suggest that the cell can exploit these differences to effect regulation.

One potential mechanism of regulation is through the microtubule-associated proteins (MAPs) that bind to microtubules, promoting their polymerization and stability (17). MAPs also spatiotemporally regulate motors by directly competing for binding to the microtubule surface, promoting or inhibiting motor attachment, or accelerating its detachment (18–23). Tau, for example, which is the most extensively studied MAP due to its involvement in many neurodegenerative diseases (24, 25), was shown to play an important role in axonal transport and was suggested to be capable of biasing

Significance

Microtubules form a network spanning the interior of cells and serve as roads for molecular motor proteins that carry organelles and other cargo to where they are needed inside the cell. The function of molecular motors is regulated for proper delivery or distribution of cargo, failure of which is linked to myriad diseases. We discovered that the microtubule-associated protein 4, which is found in cells in all tissues, can determine whether mitochondria accumulate around the nucleus or distribute throughout the cell by controlling the kinesin motor's ability to generate force, a novel mode of regulation. Our findings can guide therapeutic strategies for the paradoxical increased metastasis fueled by the spread of mitochondria in response to certain cancer treatments.

bidirectional transport toward the microtubule minus-end by differentially inhibiting the processivity of kinesin-1, kinesin-2, and dynein (18, 22, 23, 26, 27). In support of the crucial role they play in regulating transport, MAPs are highly regulated, mainly via isoform expression and phosphorylation (25, 28). The ubiquitous microtubule-associated protein 4 (MAP4) and the human tau have four and six isoforms, respectively, which differ in the number of microtubule-binding repeats and the length of the projection domain, the region of the protein that projects outward from the microtubule surface (17). The function of the projection domain of MAPs is less well studied than the microtubule-binding domain, although there are a few studies that report its role in the control of the spacing between microtubules as well as affecting motor motility on the microtubules (18, 22). The phosphorylation of tau, on the other hand, modulates the dynamic equilibrium between its static and transient binding to microtubules (25). Hence, regulation of its phosphorylation is indispensable because its aberrant phosphorylation has been linked to disease (29–32), such as Alzheimer's disease, where tau is highly phosphorylated and many of the phosphorylated sites are targeted by an abnormally hyperactive glycogen synthase kinase 3 (GSK3) (33–35).

GSK3 is a serine–threonine kinase that functions in both neuronal and nonneuronal cells and has been implicated in several cancers, neurodegenerative diseases, and diabetes (36–38). In addition to its involvement in tau regulation via phosphorylation, it also has been implicated as a regulator of kinesin-dependent axonal transport in squid and flies (39–41) and cytoplasmic dynein in both neuronal and nonneuronal cells (42). In support of a central role in regulating intracellular transport, overexpression of GSK3 in neuronal cells was shown to reduce the plus-end movement of mitochondria (43) and to negatively regulate bidirectional transport of the amyloid precursor protein (41). Furthermore, in nonneuronal cells, it was reported that GSK3 is involved in regulating the transport of the acidic organelles in young adult mouse colonic cells via dynein inhibition (42) and lipid droplets in *Drosophila* embryos by altering kinesin activity (41). It was also reported that the phosphorylation of kinesin by GSK3 leads to the motor's

detachment from the cargo in vitro (40). Although the important role that GSK3 plays in intracellular transport is well established, its mechanisms of action remain poorly understood, especially at the molecular level, and may vary for different cargoes and in different tissues.

The ubiquitous expression of GSK3 led us to study tau's structurally related nonneuronal MAP, MAP4, which is also ubiquitously expressed. MAP4 was reported to interfere with cargo trafficking (44, 45), yet the molecular mechanisms are not understood. We therefore investigated its role in transport regulation using wild-type (WT) and GSK3β knockout (GSK3β KO) mouse embryonic fibroblasts (MEFs) as a model system. Using a nonneuronal model allowed us to uncover the role and molecular mechanism of this ubiquitous MAP in regulating the directionality of organelle transport along microtubules and, notably, to identify it as a possible mediator of altered mitochondrial localization in cancer cells.

Results

Absence of GSK3β leads to MAP4 phosphorylation and perinuclear clustering. Given the well-documented role of GSK3β in phosphorylating the neuronal MAP tau, we decided to investigate whether the ubiquitous MAP4 is also a phosphorylation substrate of GSK3β in MEFs. Using phosphorylation affinity electrophoresis combined with Western blotting, we compared MAP4 phosphorylation in WT and GSK3β KO MEFs, which do not express GSK3β (*SI Appendix,* Fig. S1A). Results show a striking difference in MAP4 band migration between WT and GSK3β KO, suggesting a difference in its phosphorylation status (Fig. 1A). However, unlike tau, MAP4 becomes phosphorylated in the absence of GSK3β, suggesting that it must be a phosphorylation substrate of other kinases that are downstream of and inhibited by GSK3β.

Since the phosphorylation of tau is known to reduce its affinity to microtubules, we examined whether MAP4 phosphorylation in this case also affects its distribution within the cell. In WT MEFs, MAP4 decorates the microtubules, as can be judged by the filamentous structures it forms (Fig. 1B). On
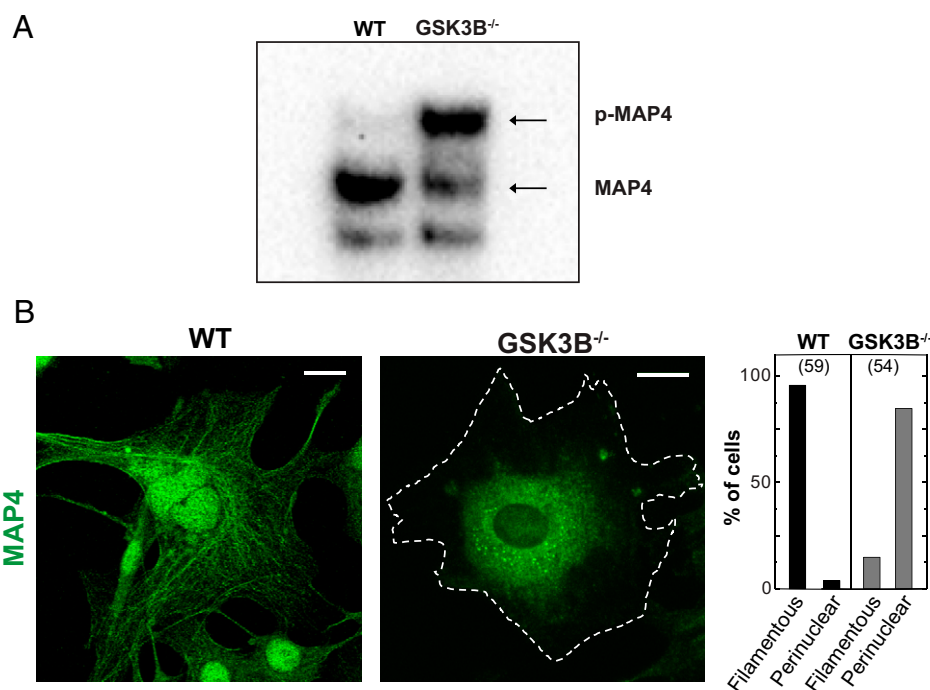
Fig. 1. Altered phosphorylation and cellular distribution of MAP4 in the absence of GSK3β. (*A*) Phosphorylation–affinity electrophoresis coupled with Western blotting for MAP4 of WT and GSK3β KO (GSK3B$^{-/-}$) MEF extracts (*n* = 3). (*B*) Representative confocal images and analysis of WT and GSK3B$^{-/-}$ MEFs immunostained for MAP4 in green (Bars, 20 μm). The number of analyzed cells is shown in parentheses.

the other hand, in the GSK3β KO MEFs, MAP4 no longer aligns with the microtubules but rather becomes perinuclearly clustered (Fig. 1*B*), despite the microtubules remaining intact in these cells (*SI Appendix*, Fig. S1*B*).

Abnormal distribution and phosphorylation of MAP4 is accompanied with perinuclear clustering of organelles. With the microtubules becoming bare of (no longer covered by) MAP4 in the GSK3β KO MEFs and knowing that tau-decorated microtubules impair kinesin-based transport (18, 22, 46–48), we initially predicted that organelles should distribute at the cell peripheries driven by unopposed kinesin transport. Surprisingly, both mitochondria and lipid droplets, known to be transported along microtubules by kinesin-1 and cytoplasmic dynein, become perinuclearly clustered in the GSK3β KO cells (Fig. 2 *A, B, E,* and *F*). This is in contrast to their WT counterparts, which are distributed throughout the whole cytoplasm (Fig. 2 *A, B, E,* and *F*). The perinuclear clustering phenotype could be rescued by overexpressing GSK3β in the KO cells (Fig. 2 *C, E,* and *F*) and phenocopied in WT cells by inhibiting GSK3β using two different pharmacological drugs, AR-A014418 and SB-216763 (Fig. 2 *D* and *E*). Taken together, these findings show that the plus-end transport of organelles is compromised in the absence of GSK3β. The striking phenotype where both organelles and MAP4 are perinuclearly clustered suggests that MAP4 phosphorylation may be playing a crucial role in the regulation of lipid droplet and mitochondrial transport in MEFs.

Kinesin-1 is active in GSK3β KO MEFs. To understand what disrupts the plus-end transport of organelles in the absence of GSK3β, we asked whether the MEF isoform of kinesin-1, KIF5B, is present and active on these cargoes. Dissociation of the motors from cargo had previously been suggested as a mechanism for transport regulation (40, 49). However, immunofluorescence images of lipid droplets purified from WT and GSK3β KO MEFs clearly show the presence of KIF5B on their surface (Fig. 3*A*), suggesting that the failed peripheral distribution is not caused by defects in motor–cargo attachment. Indeed, the distribution of KIF5B in fixed cells mirrors the distribution of lipid droplets and mitochondria, being evenly dispersed throughout the cytoplasm in WT cells while largely perinuclearly clustered in the KO cells (Fig. 3*B*). This implies that the transport of other kinesin-1 cargoes must also be compromised. Nevertheless, despite the overall impairment of plus-end transport, tracks of the few individually discernible lipid droplets at the edge of the perinuclear cluster and in sparse areas in the KO cells clearly display bidirectional motion, as they do in the WT MEFs (Fig. 3*C*), but their extent of motion is severely reduced (Fig. 3*D*). This finding indicates that kinesin that is present on the organelles is still active and can step along the microtubules in the absence of GSK3β. Kinesin's inability to distribute cargoes away from the perinuclear region must therefore result from factors that undermine its activity.

Impaired kinesin activity allows dynein to sweep organelles back. Similar to kinesin, dynein is present on lipid droplets purified from WT and GSK3β KO MEFs (Fig. 4*A*), and its activity is evident from the bidirectional trajectories of cargoes in live cells (Fig. 3 *C* and *D*). The perinuclear clustering of kinesin-1 cargoes in the absence of GSK3β despite their ability to move bidirectionally strongly suggests that dynein activity must be overwhelming that of kinesin. To test this suggestion, we inhibited dynein using the pharmacological drug ciliobrevin and measured its effect on the distribution of cargoes. With

minus-end but not plus-end transport inhibited, cargoes should spread away from the perinuclear region. Indeed, dynein inhibition rescues the perinuclear clustering of mitochondria in the KO cells (Fig. 4 *B* and *C*) and leads to the appearance of some accumulations of mitochondria at the cell peripheries in both WT and KO MEFs (Fig. 4*B*). These findings once again confirm that kinesin is active in the absence of GSK3β and demonstrate that its activity is overwhelmed by that of dynein. The perinuclear clustering would then indicate the misregulation of bidirectional transport that tips the balance in favor of minus-end transport. This can be a consequence of enhanced dynein motility, impaired kinesin motility, or both.

Because GSK3β is a kinase, we tested whether the differential regulation of motor activity could be unrelated to MAP4 phosphorylation but rather a direct consequence of phosphorylation of the motor subunits as previously reported for the kinesin heavy chain, kinesin light chain 2 and the dynein intermediate chains (14, 40, 42). We therefore examined the phosphorylation status of these subunits using phosphorylation affinity electrophoresis combined with Western blotting. Neither showed a difference in the phosphorylation status between WT and GSK3β KO cells (*SI Appendix*, Fig. S2), excluding a direct role for the phosphorylation of these subunits in the differential regulation of the opposite polarity motors by GSK3β.

MAP4 associates with cargoes and binds to the dynein/dynactin complex. The phosphorylation of MAP4 in the absence of GSK3β suggests that MAP4 may be directly interfering with kinesin function in a phosphorylation-dependent manner, hence resulting in the observed perinuclear clustering of organelles. To test this hypothesis, we used a single-molecule in vitro assay to study kinesin motility on microtubules decorated with MAP4 purified from WT nontreated cells and cells treated with the GSK3β inhibitor, LiCl. In both cases, MAP4 reduced kinesin's run length and its ability to bind the microtubules (*SI Appendix*, Fig. S3), which is consistent with previous findings for MAP4 (50) and other MAPs (22, 27, 47). However, contrary to our expectation and inconsistent with our finding that plus-end transport is compromised in the GSK3β KO MEFs, MAP4 from LiCl-treated cells had a slightly weaker effect on kinesin. These results suggest that the observed perinuclear clustering of organelles in the absence of GSK3β cannot be solely caused by the change in the phosphorylation state of MAP4 decorating the microtubules.

Nevertheless, a role for MAP4 in regulating the distribution of the organelles can be gleaned from the observation that both MAP4 and the organelles are perinuclearly clustered in the KO cells, suggesting that they may colocalize. Indeed, upon close inspection of immunofluorescence images in the KO cells, we find that MAP4 displays punctate structures that resemble cargoes (Fig. 1*B*). To check whether these structures are due to MAP4 association with the organelles, we costained the cells for MAP4 as well as mitochondria and lipid droplets. We found that not only does the distribution of MAP4 mirror the distribution of both cargoes, but zooming in on individual isolated mitochondria or lipid droplets also shows MAP4 decorating their surface (Fig. 5*A*). Furthermore, images of immunostained purified lipid droplets clearly show an enrichment of MAP4 on the surface of the droplets isolated from GSK3β KO MEFs (Fig. 5*B*). These results were further confirmed by Western blotting performed on the purified lipid droplets, which demonstrates a significant increase in MAP4 in the lipid droplets sample isolated from the GSK3β KO MEFs (Fig. 5*C*). Taken together, these results confirm that upon its phosphorylation, MAP4 associates with motor
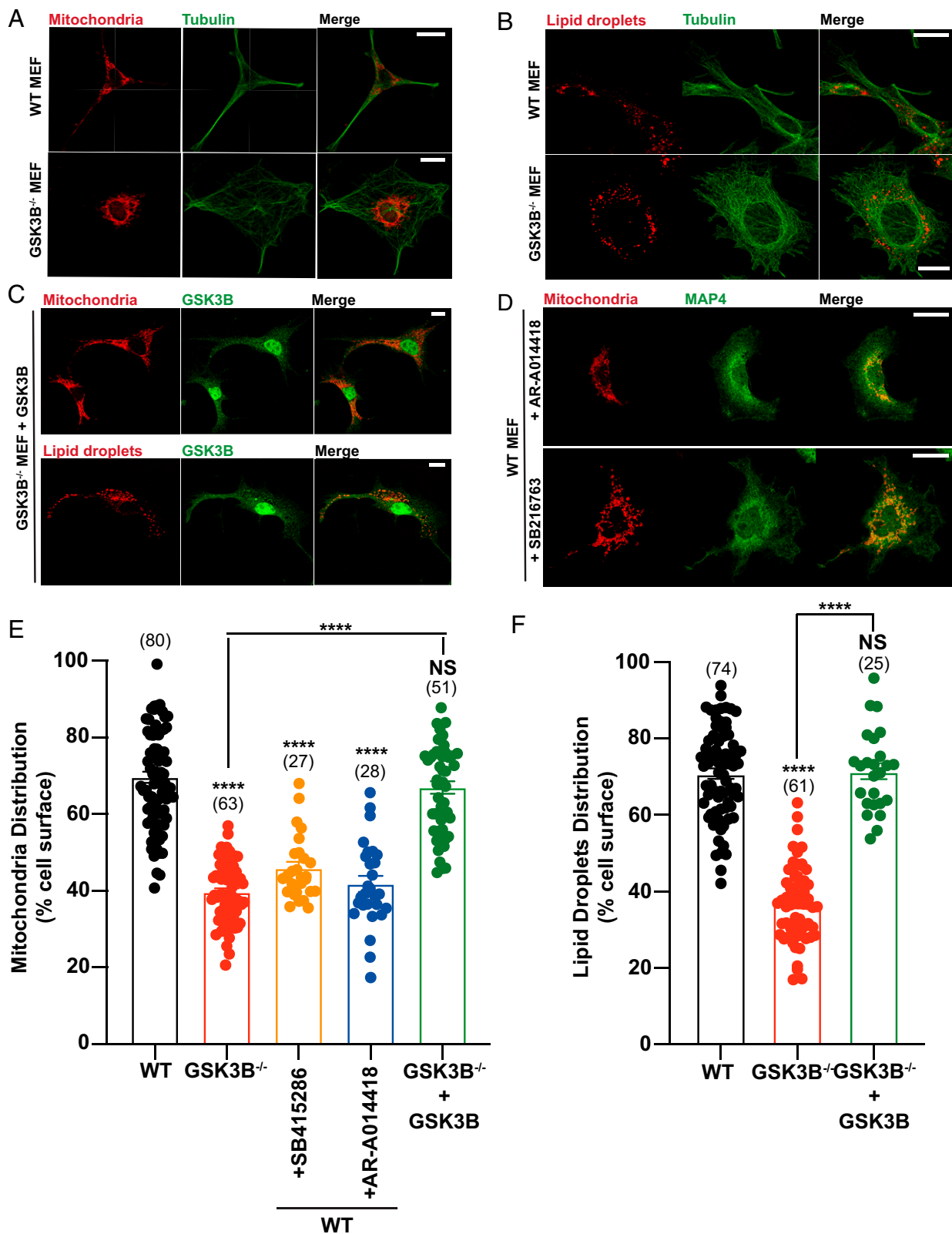
Fig. 2. Perinuclear clustering of mitochondria and lipid droplets in the absence of GSK3β. Representative images of WT and GSK3β KO (GSK3B$^{-/-}$) MEFs immunostained for microtubules in green and mitochondria (*A*) or lipid droplets (*B*) in red. (*C*) Representative example of mitochondria/lipid droplets rescued distribution in GSK3β KO MEF upon GSK3β overexpression. Mitochondria/lipid droplets are shown in red and GSK3β in green. (*D*) Representative confocal images of WT MEF showing perinuclear clustering of mitochondria and MAP4 upon treatment with the GSK3β inhibitors AR-A014418 or SB216763. Mitochondria are shown in red and MAP4 in green (Bars, 20 μm). (*E*) Analysis of mitochondria distribution, represented here as percentage of cell surface area, in WT MEFs in the absence or presence of the GSK3β inhibitors SB415286 and AR-A014418, and in GSK3β KO MEFs before and after the overexpression of GSK3β. (*F*) Analysis of lipid droplet distribution in WT MEFs and GSK3β KO MEFs before and after overexpression of GSK3β. In (*E*) and (*F*), results were compared with WT or to each other where indicated and expressed as mean ± SEM; $^{NS}P > 0.05$ and $****P < 0.0001$. NS, not significant. The number of analyzed cells is shown in parentheses.
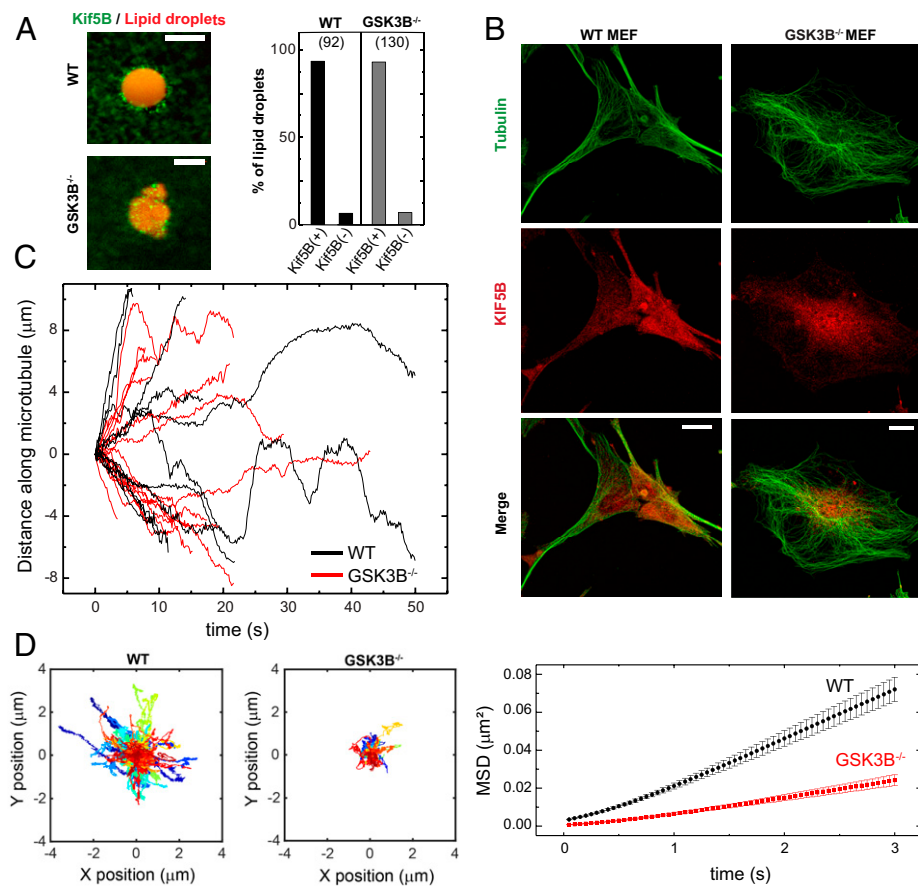
Fig. 3. Kinesin is present on the organelles and still engages in bidirectional transport in the absence of GSK3β. (*A*) Representative example and analysis of lipid droplets isolated from WT and GSK3β KO MEFs labeled in red with Nile Red and immunostained for kinesin 1 (KIF5B) in green (Bars, 5 µm). The number of analyzed lipid droplets is shown in parentheses. KIF5B(+) and KIF5B(-) droplets display KIF5B staining, or no staining, respectively. (*B*) Representative confocal images of WT and GSK3β KO MEFs immunostained for KIF5B in red and microtubules in green (Bars, 20 µm). (*C*) Tracks of Nile Red–labeled lipid droplets moving along microtubules in WT and GSK3β KO MEFs. Data are presented as distance traveled by the individual droplets along microtubules, with positive slope representing movements toward the plus-end of microtubules and negative slopes toward the minus-end. (*D*) Tracks of Nile Red–labeled lipid droplets in WT and GSK3β KO cells represented with the initial position set at the origin to highlight the reduced extent of organelle travel in the KO cells as also evident in the mean square displacement (MSD) analysis.

cargoes, hence remaining in the perinuclear region rather than decorating the length of the microtubules. They also imply that the mechanism by which MAP4 regulates motor-based transport could be distinct from that of tau and requires its association with the organelles.

We next set out to identify what MAP4 interacts with on the organelles. To that end, extracts from WT and GSK3β KO cells were used for immunoprecipitation (IP) assay using an anti-MAP4 antibody. The IP samples were then analyzed using Western blotting and mass spectrometry. Among the many peptides that were found to interact with MAP4, we identified different subunits of dynein and its cofactor the dynactin complex, but not kinesin, in both WT and GSK3β KO extracts (Fig. 5 *D* and *E*). These results suggest that MAP4 may bind to the surface of motor cargoes via a direct interaction with the dynein/dynactin complex. However, our finding that MAP4 interacts with the dynein/dynactin complex in both WT and GSK3β KO cells does not explain its propensity to associate with organelles in the latter. It is possible, therefore, that the phosphorylation of MAP4 in the GSK3β KO cells reduces its affinity to the microtubules, leading to the interaction with the cargo–motor complex to dominate. Conversely, phosphorylation may stabilize the MAP4 association with the motor complex leading to a more pronounced accumulation of MAP4 on the organelles.

Projection domain of MAP4 is required for its association with organelles. MAP4 is a large protein, consisting of 1,125 amino acids and two major domains: at the C terminus, the microtubule binding domain (MBD), through which it binds to the microtubules, and at the N terminus, the projection domain (P-domain), whose function is still not very well understood

(Fig. 6). Having demonstrated that MAP4 binds to the surface of organelles in the absence of GSK3β, we set out to determine which part of the protein is required for such an interaction. We therefore cloned the full-length MAP4 as well as its two domains (MBD and P-domain) into green fluorescent protein (GFP)-tagged expression vectors, which were then overexpressed in WT and GSK3β KO MEFs, and their distribution within the cell was examined using confocal microscopy (Fig. 6).

The full-length MAP4-GFP, when transfected into cells, shows a distribution similar to that of the endogenous MAP4. In the WT MEFs the protein forms filamentous structures tracing microtubules, whereas it becomes perinuclearly clustered and punctate in the GSK3β KO cells (Fig. 6*A*), suggesting its association with cargoes. Overexpression of MBD-GFP, however, shows the same filamentous structures in both the WT and GSK3β KO cells (Fig. 6*B*). These findings suggest that the microtubule-binding domain of MAP4 is still capable of binding the microtubules in the absence of GSK3β. Moreover, they indicate that the missing projection domain must be playing an important role in the association of full-length MAP4 with cargoes in the KO cells.

To further confirm this finding and further understand the mechanism by which MAP4 associates with the organelles, the GFP-tagged P-domain was overexpressed in WT and GSK3β KO MEFs. Images of the WT cells transfected with P-domain-GFP show a diffuse signal (Fig. 6*C*), suggesting that in the absence of the MBD, MAP4 is no longer capable of interacting with the microtubules. In the GSK3β KO cells, however, P-domain-GFP is no longer perinuclear although it still forms the punctate structures (Fig. 6*C*), an indication of its association with cargoes. These findings confirm that MAP4 interaction with
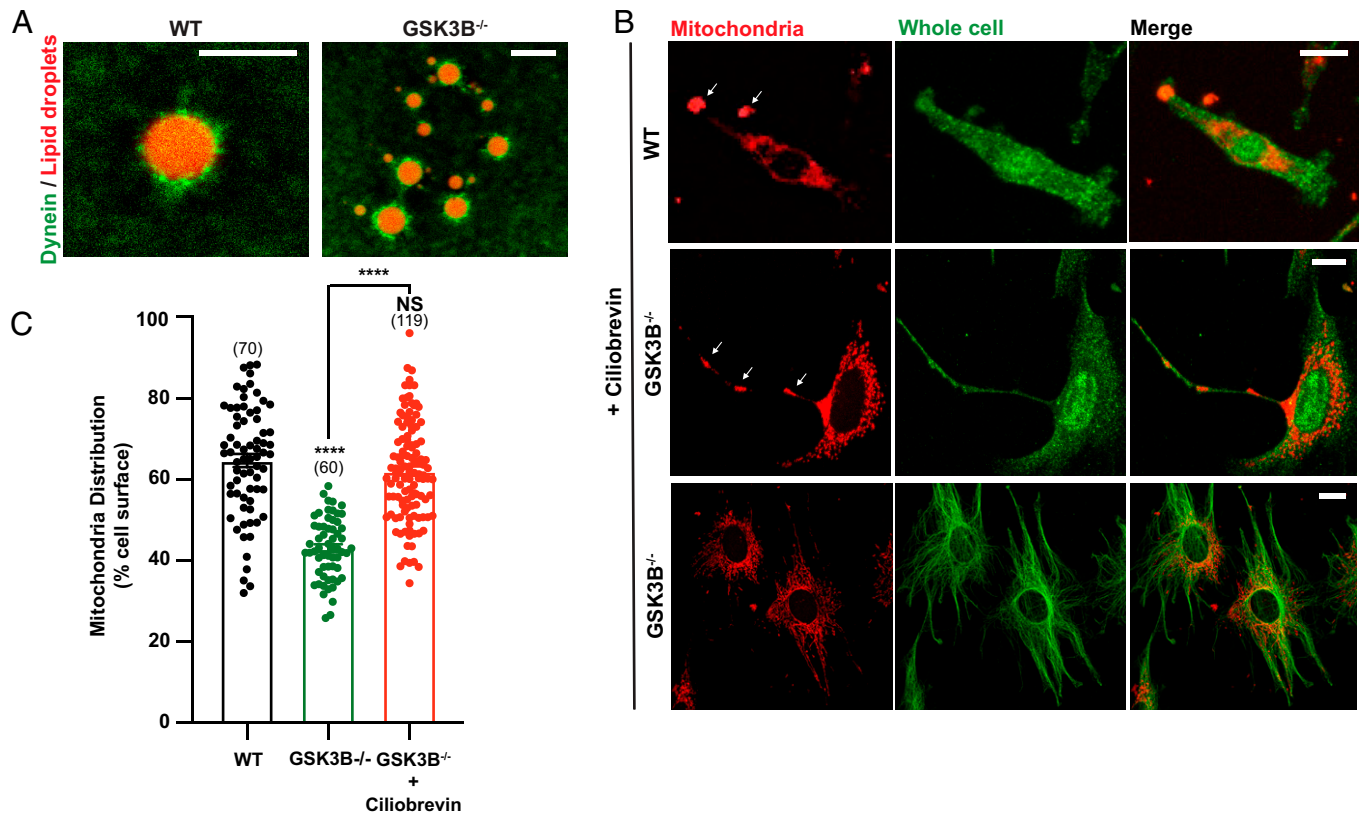
Fig. 4. Inhibition of dynein rescues the perinuclear clustering of cargoes in GSK3β KO cells. (*A*) Representative example of lipid droplets isolated from WT and GSK3β KO MEFs labeled in red with Nile Red and immunostained for cytoplasmic dynein in green (Bars, 5 μm). (*B*) Representative confocal images of WT and GSK3β KO MEFs showing mitochondria distribution upon treatment with the dynein inhibitor ciliobrevin. Mitochondria are shown in red and the green channel is used as a visual guide to outline the cell (MAP4 in the top two images, and tubulin in the bottom one). The arrows point toward peripheral accumulations of mitochondria in both WT and GSK3β KO MEFs upon dynein inhibition (Bars, 20 μm). (*C*) Analysis of mitochondria distribution, represented here as percentage of cell surface area, in WT MEFs and GSK3β KO MEFs in the presence or absence of ciliobrevin. Results were compared with WT or to each other where indicated and expressed as mean ± SEM; [NS]$P > 0.05$ and [****]$P < 0.0001$. The number of analyzed cells is shown in parentheses.

cargoes requires its P-domain and suggest that MAP4 can still bind microtubules in the GSK3β KO cells. Furthermore, had a potential reduction in the affinity of phosphorylated MAP4 to microtubules been behind its preferential association with the cargoes, the overexpressed projection domain would distribute similarly in both WT and GSK3β KO cells, since it does not bind the microtubules. Instead, phosphorylation is likely acting to stabilize the MAP4 association with the organelles. Consistent with this, the P-domain of MAP4 but not the MBD is phosphorylated in the KO cells (*SI Appendix*, Fig. S4). Taken together, all these results imply that the full-length MAP4 must be interacting with both microtubules and cargo via its MBD and phosphorylated P-domain respectively, hence tethering cargoes to microtubules in the absence of GSK3β.

Tethering the organelles to the microtubule via phosphorylated MAP4 is required for the perinuclear clustering of organelles. We next asked whether tethering the organelles to microtubules via MAP4 might underlie the perinuclear clustering of cargoes in the GSK3β KO MEFs. The prediction, then, would be that eliminating this tether should rescue the phenotype. We reasoned that overexpressing either the MBD or the P-domain of MAP4 should compete with the binding sites of endogenous MAP4, reducing its propensity to form the tether. We therefore examined the distribution of cargoes in cells where exogenous MAP4 MBD or P-domain were overexpressed. Indeed, we found that the perinuclear distribution of mitochondria in the GSK3β KO cells is rescued in both cases (Fig. 7 *A* and *B*). Notably, such a rescue was not observed when the GSK3β KO cells

were transfected with full-length MAP4-GFP (Fig. 7 *A* and *B*). These results confirm that the perinuclear clustering of cargoes requires the simultaneous action of both domains of MAP4 and suggests that the MAP4 tether between the organelle and the microtubule may be biasing the bidirectional transport of the organelles toward the microtubules minus-end. This could happen, for instance, by the tether exerting a hindering force that would differentially impair kinesin, known to be more prone to detachment when hindered than dynein (6, 15). Alternatively, extending MAP4 could position it in a conformation that enables it to interact with kinesin and impair its function.

To differentiate between these two models, we designed an in vitro bead motility assay where truncated kinesin (K560) and MAP4 were simultaneously and specifically bound to the beads to mimic the in vivo configuration. In vitro, these beads exhibit intermittent long-range motion along the microtubules interrupted by short pauses and recoils (Fig. 7*C*), suggesting that the bead-bound MAP4 also attaches to the microtubules, forming a tether. The ability of bead-bound MAP4 to tether the bead to the microtubule was confirmed using beads lacking kinesin, which still attach to the microtubule but exhibit short-range diffusive motion as opposed to the directed motion observed in the presence of kinesin (*SI Appendix*, Fig. S5). We next used optical tweezers to measure force generation. In the absence of kinesin, less than 1 pN of force is sufficient to suppress MAP4 diffusion along the microtubule, and the beads are easily dragged along the microtubule by the weak optical trap. Conversely, in the absence of MAP4 on the beads, kinesin can sustain forces that are typically
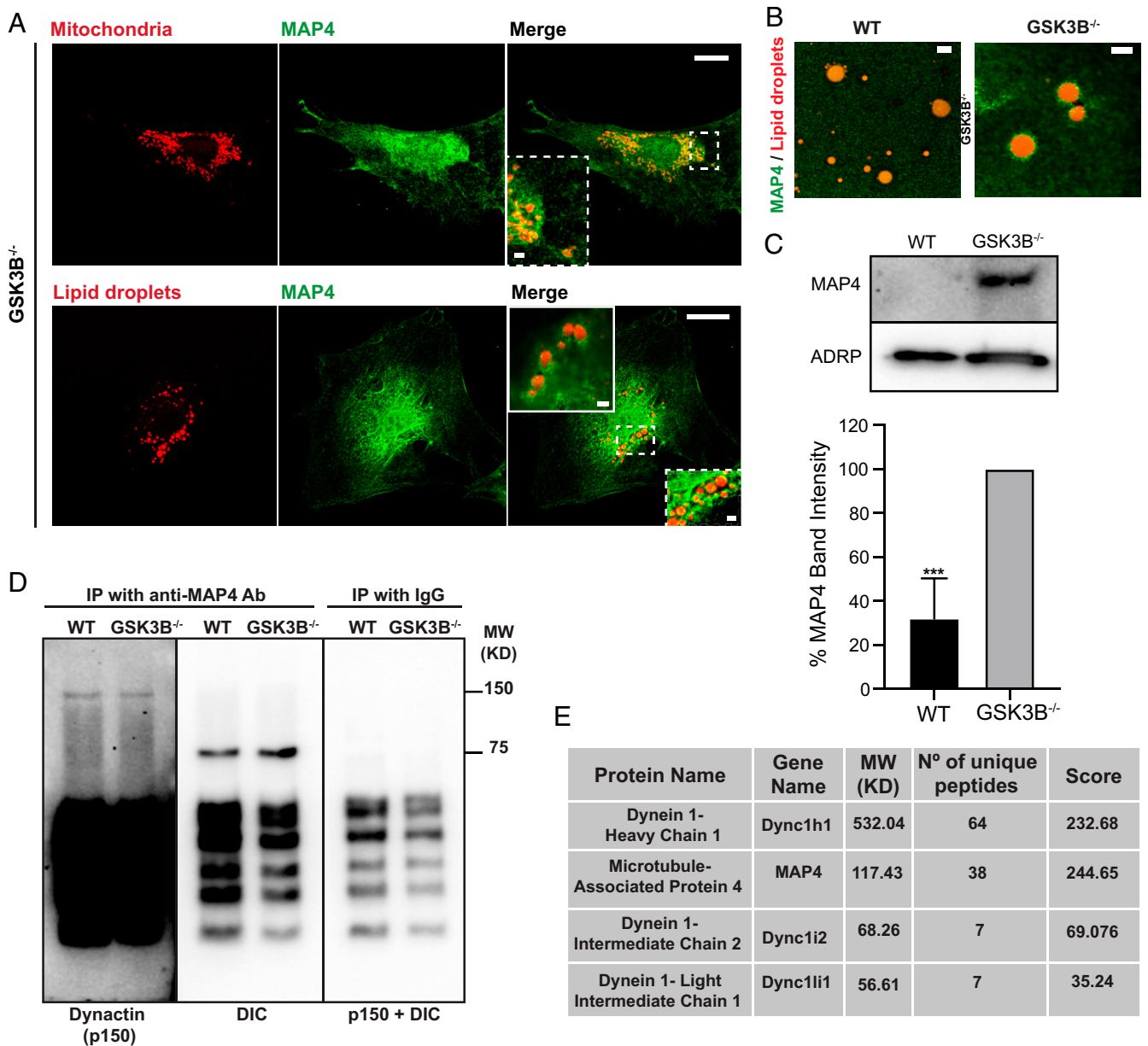
Fig. 5. MAP4 accumulates on the organelles in the absence of GSK3β and physically interacts with the dynein/dynactin complex. (*A*) Representative images of GSK3β KO MEFs immunostained for MAP4 in green and mitochondria or lipid droplets in red (Bars, 20 μm). The magnified insets show examples of MAP4 colocalizing with individual organelles and decorating the surface of lipid droplets (Bars in insets, 2 μm). (*B*) Representative example of lipid droplets isolated from WT and GSK3β KO MEFs labeled in red with Nile Red and immunostained for MAP4 in green (Bars, 5 μm). (*C*) Western blot and densitometric analysis of the lipid droplet fraction from WT and GSK3β KO cell extracts probed for MAP4 (*n* = 3). ADRP was used as a loading control. Results are mean ± SEM; ***P < 0.001. (*D*) Western blot of WT and GSK3β KO MEFs immunoprecipitates using anti-MAP4 antibody or IgG (*n* = 3), probed with antibodies against dynactin (p150) and dynein intermediate chains (DIC). (*E*) Mass-spectrometry analysis of WT and GSK3β KO MEF immunoprecipitates using anti-MAP4 antibody. Results confirm MAP4 interaction with different subunits of dynein.

approximately 5pN (Fig. 7 *D* and *E*), as previously reported for the motor (51). The typical force that the motor can sustain significantly drops in the presence of MAP4 (Fig. 7 *D* and *E*), suggesting that MAP4 indeed hinders kinesin's capacity to generate force, which is a prerequisite for its ability to transport organelles in cells. Notably, bead-bound MAP4 purified from cells where GSK3β was inhibited using LiCl resulted in a more drastic reduction of kinesin's force generation (to approximately 2.4 pN) than MAP4 purified from untreated cells (Fig. 7 *D* and *E*), highlighting the importance of the phosphorylation state of MAP4. In the absence of kinesin, MAP4 purified from the GSK3β-inhibited cells could still tether the beads to the microtubules and was readily pulled along the microtubule using the weak optical trap (*SI Appendix,* Fig. S5). Furthermore, eliminating the MAP4 tether by only decorating the microtubules (but not the beads) with MAP4 purified from GSK3β-inhibited cells only marginally reduces kinesin's capacity to sustain force (Fig. 7*E*), indicating that MAP4 binding to both the bead and the microtubule is necessary for its effect to strongly decrease kinesin's force production. Taken together, these in vitro findings strongly support the conclusion based on the in vivo results that when simultaneously bound to both microtubules and organelles, phosphorylated MAP4 hinders kinesin's ability to move the organelles, resulting in their perinuclear accumulation. The findings further support a model in which extending phosphorylated MAP4 between the cargo and the microtubule positions it to interact with kinesin and undermine its function.
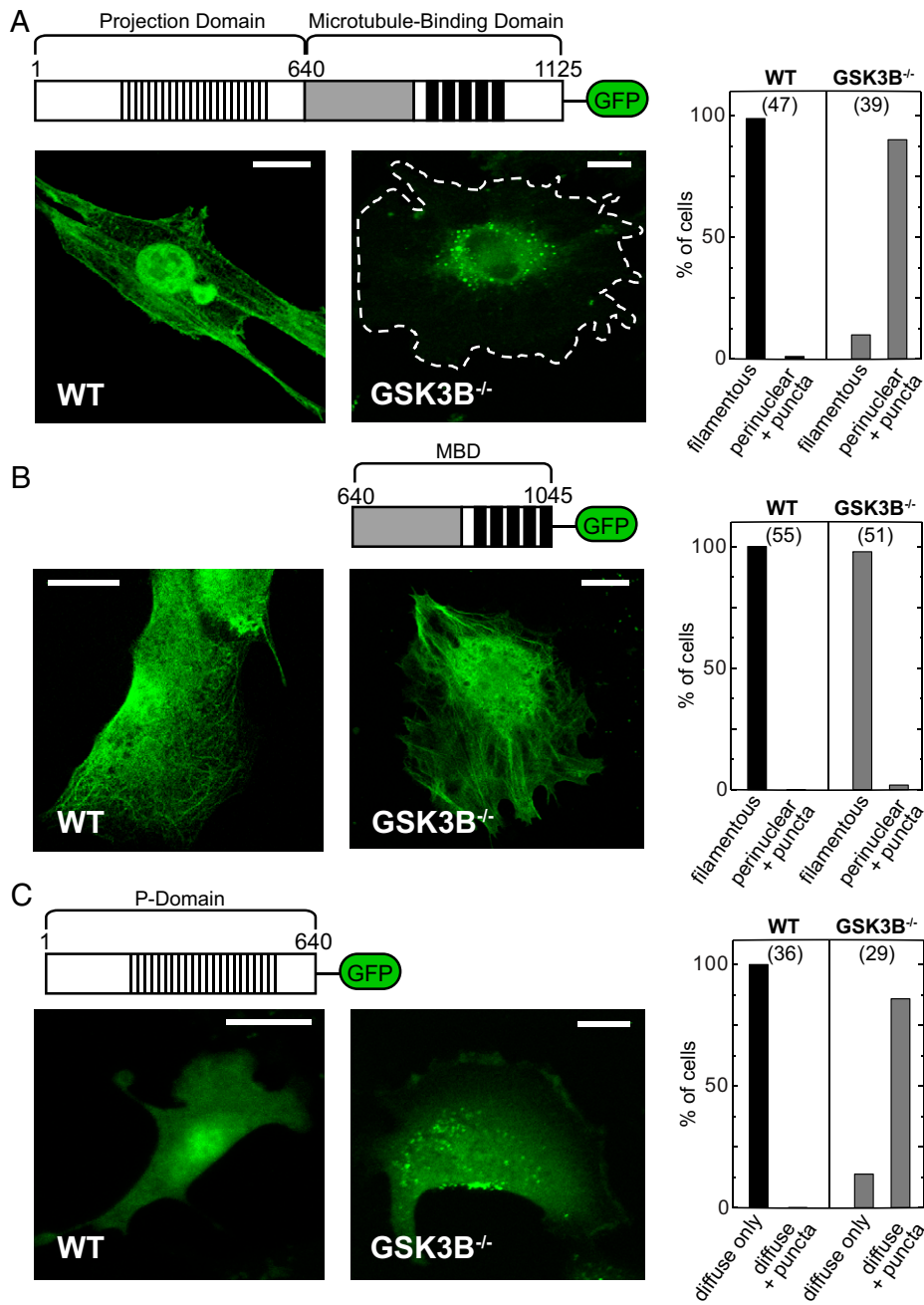
Fig. 6. The projection domain is responsible for MAP4's association with cargoes. Representative images and quantitative analysis of WT and GSK3β KO (GSK3β$^{-/-}$) MEFs transfected with vectors expressing GFP-tagged full-length MAP4 (A), MBD (B), or P-domain (C) (Bars, 20 µm). Puncta, punctate. The number of analyzed cells is shown in parentheses.

MAP4 localization mirrors the perinuclear clustering of mitochondria in the A549 cancer cell line. We next asked whether our findings can provide an explanation for the reported perinuclear clustering of mitochondria in various cancer cells (52). In those cells, it was shown that small-molecule antagonists of the universal tumor driver phosphatidylinositol 3-kinase (PI3K) pathway lead to mitochondrial dispersal away from the nucleus. PI3K activity is known to inhibit GSK3β (53). Therefore, we hypothesized that the perinuclear clustering of mitochondria in the untreated cancer cells might be driven by the same MAP4-related mechanism we identified in GSK3β KO cells. In the GSK3β KO cells, we observed perinuclear clustering of MAP4 that mirrors the distribution of the organelles, both for endogenous and overexpressed full-length MAP4 (Figs. 1B, 5A, and 6A). We therefore examined MAP4 distribution in lung carcinoma epithelial cells, A549, which were previously shown to exhibit perinuclear clustering of mitochondria (52). Immunofluorescence images of A549 cells show that MAP4 is perinuclear and

that its distribution largely follows the perinuclear distribution of mitochondria (Fig. 8). This is consistent with MAP4 playing a role in the clustering of the mitochondria in the same fashion it does in the GSK3 KO cells and has implications on treatment strategies, as discussed in the next section.

Discussion

The regulation of cargo directionality along the microtubules determines proper delivery and cargo distribution. The molecular details of how the cell achieves this regulation for various cargo types are likely multifaceted and can in principle involve all the components of the transport machinery, but they remain poorly understood. Here, we have shown that the microtubule-associated protein 4 (MAP4) can play a direct role in biasing cargo transport toward the minus-ends of microtubules in a phosphorylation-dependent manner. The association of MAP4 with the dynein machinery may suggest an enhancement of
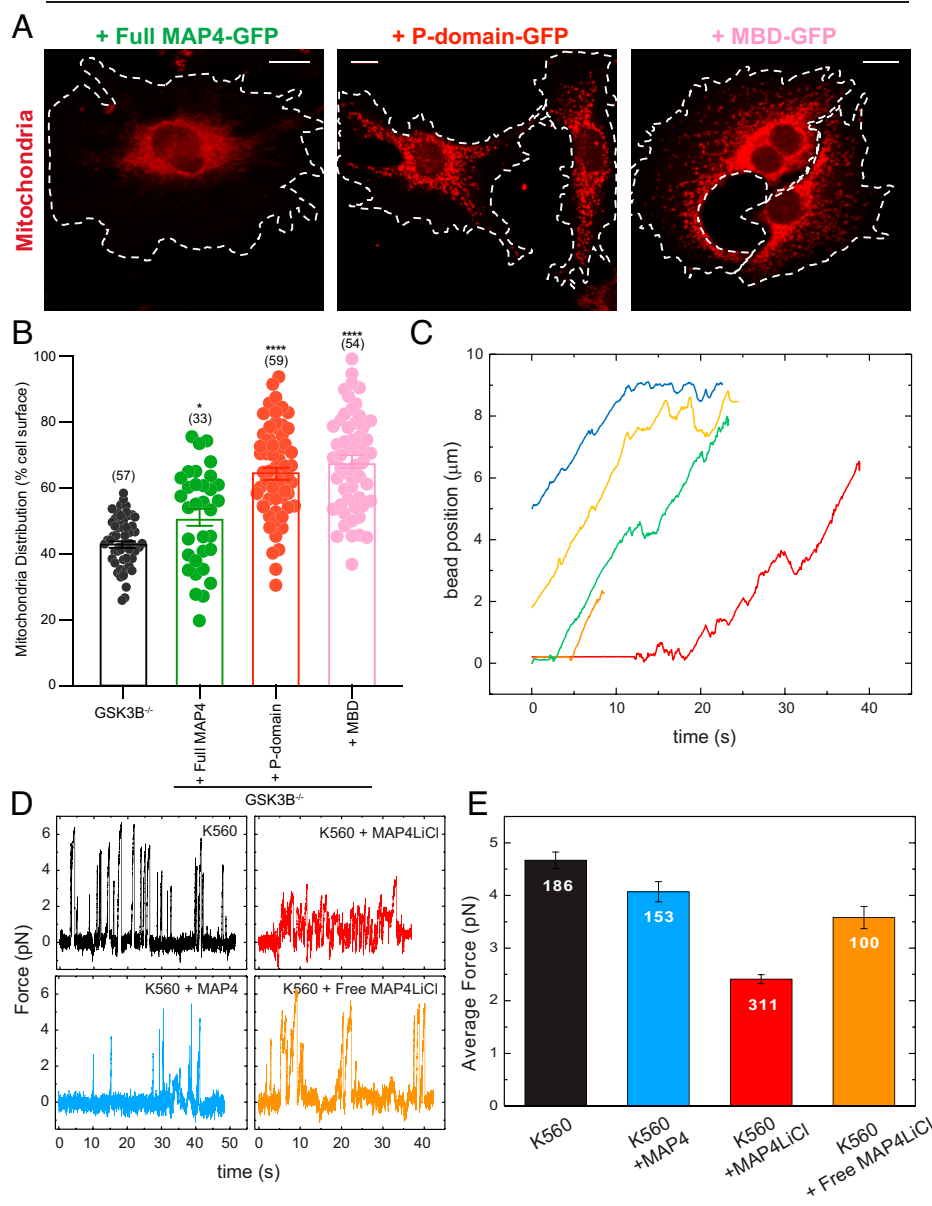
Fig. 7. MAP4 simultaneous binding to both microtubules and organelles is required for their perinuclear clustering. Representative images (*A*) and data analysis (*B*) of the distribution of mitochondria in GSK3β KO MEFs and GSK3β KO overexpressing GFP-tagged full-length MAP4 (Full MAP4-GFP), P-domain-GFP, or MBD (MBD-GFP) (Bars, 20 μm). In (*B*), results were compared with GSK3β KO and expressed as mean ± SEM; ******P* < 0.05 and *********P* < 0.0001. The number of analyzed cells is shown in parentheses. (*C*) In vitro trajectories along microtubules of beads decorated with both kinesin (K560) and MAP4 showing frequent recoils and pauses. (*D*) Force generation by beads trapped using optical tweezers in proximity of a microtubule. The beads were decorated with either K560 only, K560 and MAP4 purified from nontreated cells (K560+MAP4), K560 and MAP4LiCl (K560+MAP4LiCl), or K560 only with MAP4LiCl decorating the microtubules but not the beads (K560+ Free MAP4LiCl). (*E*) The mean peak force before detachment and recoil to the trap center measured for beads decorated with K560, K560 and MAP4, K560 and MAP4LiCl, or K560 only in the presence of MAP4LiCl decorating the microtubules but not the beads (K560 + Free MAP4LiCl). The number of events analyzed is indicated for each case.

dynein activity triggered by this interaction, which would be consistent with the perinuclear clustering of organelles. However, this simple model would be inconsistent with previous reports of a negative effect of MAP4 on dynein motility (20, 45). MAP4 was previously shown to slow down microtubules in an in vitro gliding assay driven by dynein/dynactin (20) and to shorten the minus-end runs of melanosomes (45). Rather, our findings paint a more elaborate molecular mechanism, consistent with previous reports, by which MAP4 biases cargo directionality in favor of dynein. The distribution of the overexpressed MAP4 projection domain and the microtubule-binding domain suggests that they compete with the full-length endogenous MAP4 for binding sites on cargoes and microtubules, respectively. Since the overexpression of each domain separately is sufficient to rescue the perinuclear clustering phenotype, we conclude that tethering the cargoes to the microtubules via the full-length MAP4 must be at the origin of the perinuclear clustering of cargoes. The formation of this tether may therefore differentially interfere with the ability of kinesin

and dynein to transport the cargoes by opposing their force generation.

The reaction of kinesin and dynein to opposing forces has been previously mapped out in detail and found to be distinct for the two motors. While dynein is tenacious, displays catch-bond–like interaction with the microtubules, and can enhance its force production in response to load, kinesin detaches quickly when opposed (6, 15, 16, 54). In the GSK3β KO cells, the MAP4 tether would then lead to failed attempts by kinesin to move the cargoes long distances but would not compromise dynein. This biases the bidirectionally moving cargoes toward the minus-ends of microtubules, clustering them perinuclearly. The in vitro optical tweezer measurements (Fig. 7*E*) suggest that this mechanism can only partially explain the perinuclear clustering. While MAP4 association with the organelles is a prerequisite for their accumulation in the nuclear region, the in vitro measurements indicate that MAP4 binding the organelle and microtubule simultaneously is not sufficient. More pronounced impairment of kinesin force generation requires
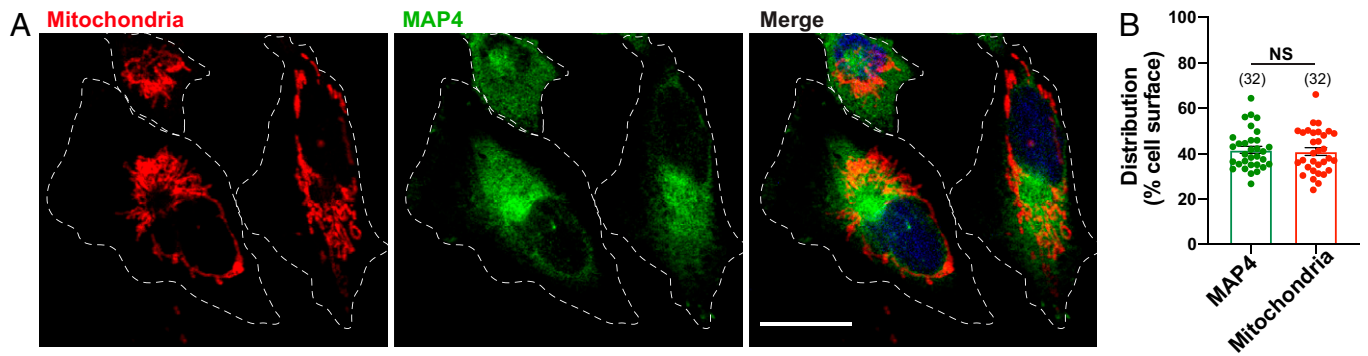
Fig. 8. MAP4 distribution mirrors the perinuclear localization of mitochondria in the A549 cancer cell line. Representative images (*A*) and data analysis (*B*) of the distribution of mitochondria (red) and MAP4 (green) in A549 cancer cells. DNA is stained in blue (Scale bars, 20 μm). Results were expressed as mean ± SEM; $^{NS}P > 0.05$. The number of analyzed cells is shown in parentheses.

altering MAP4 phosphorylation. Therefore, in cells, phosphorylation of MAP4 leads it to both associate with organelles and interact with kinesin, compromising its ability to generate force. Similarly, both the cell and in vitro measurements show that phosphorylation of MAP4 alone is not sufficient to impair kinesin but rather that phosphorylation needs to be accompanied by MAP4 binding to both the cargo and the microtubule simultaneously. The overexpression of the projection domain of MAP4 in the GSK3β KO cells leads to it associating with the organelles, just like the phosphorylated full-length endogenous MAP4, yet it cannot impair kinesin since the projection domain does not bind the microtubule. In vitro, the presence of the phosphorylated MAP4 on the microtubules does not considerably impair kinesin's force generation unless it also binds the beads. Finally, in vitro, we find that MAP4-tethered beads slide easily along microtubules in the absence of kinesin, so drag from the MAP4 tether cannot fully account for the decreased kinesin force production.

Put together, these findings paint a model in which the phosphorylation of MAP4 allows it to associate with the organelle and microtubule simultaneously. This extended conformation of phosphorylated MAP4 allows it to interact with kinesin and impair its capacity to generate force, leading dynein to sweep the organelles back. In this model, inhibiting dynein function would remove this bias and allow kinesin to inch along, albeit not efficiently due to the impaired force generation, which is consistent with the rescue of the perinuclear clustering we observed (Fig. 4). This ratcheting effect of MAP4 that favors minus-end transport in a phosphorylation-dependent manner could be distinct from and possibly in addition to the negative regulation of both kinesin-1 and dynein transport measured in vitro here and in previous reports (20, 50). Furthermore, the projection domain was not always present in these studies (50), and models based on motor-MAP4 competition for microtubule binding have been proposed (55). The requirement of both the projection and microtubule-binding domains that we found is necessary for the ratcheting mechanism of MAP4 strongly points to a distinct mechanism. Based on the data, one of course cannot exclude alternative models by which binding to both the microtubule and the dynein machinery simultaneously is a prerequisite to reducing kinesin's effectiveness in hauling cargo. For example, one could imagine that the binding of the projection domain to the cargo–motor complex increases the local concentration of MAP4 around the cargo, which would more effectively impair kinesin. However, this model would necessitate that the microtubule binding domain of MAP4 on its own not be sufficient

to impair kinesin, since overexpressing that domain, which effectively increases MAP4 concentration, rescues perinuclear clustering. Furthermore, it is not evident how MAP4 would bias transport to the minus-end in this model, since dynein transport was also shown to be impaired by MAP4 (20) and would be expected to similarly suffer from the local increase in MAP4 concentration. Further work will be needed to differentiate between these models.

Our findings highlight the central role that the projection domain of MAP4 plays in regulating microtubule-based transport. The projection domains of MAPs have so far largely been considered to serve the role of an unstructured protein brush or spacer, sterically inhibiting protein–microtubule interactions or keeping microtubules apart (17). Emerging evidence of specific binding of the projection domain of MAPs to parts of the motor complex suggest that this unstructured domain can be more than a steric brush (19, 56). A prime example is the role of MAP7 binding in the recruitment and activation of kinesin-1 (19). This nascent paradigm is bolstered by our observation that signaling by phosphorylation can modulate the interaction of MAP4 with the cargo–motor complex, resulting in a system that can regulate organelle directionality while keeping the motors bound to the organelle.

It has been suggested for quite some time that MAPs may somehow regulate transport; however, clear examples of them doing so are sparse. Here, they are directly responsible for dramatically changing the distribution of organelles in the cell, and we explain how they do so mechanically. Further, MAPs have been thought of as entirely acting on the microtubules. The idea that they can switch, as we demonstrate, and span the cargo–microtubule distance, and that this change is crucial for altering motor function, is significant. On a more mechanistic level, the notion that MAPs can result in tuning *single* motor force production quite substantially, and not due to motors simply falling off, but rather by modulation of the motor's actual force production, adds another mechanism to the repertoire of motor regulation modalities. MAP4 is ubiquitously expressed and is a major player; it is a central MAP, just as GSK3β is a very important kinase. The role and mechanism we identify for both of them is therefore expected to have broad implications, with cancer ramifications.

Indeed, our findings may provide an explanation for the observed increase in tumor cell invasive ability in response to some clinical drugs. In addition to its involvement in neurodegenerative diseases, the misregulation of GSK3β activity has been implicated in many cancers and was suggested as a metastasis-regulating factor (36, 37). Cell migration and invasion

in metastasis is energetically costly and requires the active shuttling of mitochondria to the lamellipodia at the leading edge of cells to increase the local adenosine triphosphate (ATP) concentration (57). Our finding that mitochondria are restricted to the perinuclear region in the GSK3β KO and A549 cancer cells and that MAP4 mirrors that distribution may provide the mechanism by which tumor cell invasion is paradoxically fueled by some anticancer drugs currently in the clinic. For example, the oncogenic PI3K/AKT kinase pathway is an important therapeutic target; it also inhibits GSK3 through phosphorylation. Clinically used inhibitors of the PI3K/AKT pathway lead to increased tumor cell motility and invasion that have been linked to the redistribution of energetically active mitochondria to the cortical cytoskeleton (52). Our finding that MAP4 phosphorylation in the absence of GSK3β leads to the sequestration of mitochondria around the nucleus could provide an alternative therapeutic strategy by simultaneously targeting PI3K and GSK3β to mitigate the unintended adverse effect of treatment that results in the increased metastatic potential of tumor cells.

Materials and Methods

Detailed materials and methods are included in *SI Appendix*.

Mitochondria and lipid droplets staining. Cells grown on glass coverslips in 24-well plates were incubated at 37 °C in culture media supplement with 100 nM MitoTracker Deep Red FM (M22426, Molecular Probes, Invitrogen) for 30 min or 1 µg/mL Nile Red (N1142, Thermo Fisher Scientific) for 10 min. Cells were then washed with culture media.

Tracking lipid droplet trajectories in live cells. Live MEFs grown on a glass-bottomed dish were stained for lipid droplets using Nile Red, as described above, and imaged at 37 °C using either a confocal microscope at 7 fps (Fig. 3*C*) or an epifluorescence microscope at 30 fps (Fig. 3*D*). Because the lipid droplets were perinuclearly clustered in the GSK3β KO cells, many were not individually discernible for extended periods of time. However, the few at the periphery of the cluster or in sparse areas were possible to track manually using a custom tracking program (58). To reduce the selection bias in choosing droplets with lengthy tracks at the edge of the cluster, automatic tracking using SVI's Huygens Professional was used to calculate the MSD in Fig. 3*D*.

Single-molecule in vitro motility assay. Sample chambers were constructed using polylysine-coated 0.17-mm thick coverslips and 50 µm double-sided adhesive tape as reported previously for in vitro kinesin motility experiments (54), with one exception. Two sample chambers with preassembled microtubules were constructed on the same coverslip for simultaneous assaying of truncated GFP-labeled kinesin (k560-GFP) motility in the presence of MAP4 and, as a control, k560-GFP motility in the presence of only the dialysis buffer used for MAP4 purification. This procedure was adopted to ensure similar activity and levels of kinesin in the MAP4 and control chambers. A new aliquot of k560-GFP was thawed for each measurement lasting less than 30 min from thawing. Side-by-side experiments were carried out using the same aliquot of k560-GFP almost simultaneously (2,000 frames each at 5 fps). k560-GFP was diluted in motility assay buffer (70 mM PIPEs, 4 mM EGTA, 4 mM MgSO₄, 0.1 mM EDTA, 10 mM

DTT, 20 mm taxol, 60 mM CH3COOK, and 2 mM ATP) and/or dialysis buffer (exchanged buffer from MAP4 dialysis) depending on the experiment. For each experiment, approximately equal numbers of k560-GFP motors derived from the same aliquot at optimum concentration were incubated with MAP4 and MAP4 dialysis buffer. The incubation lasted for 5 min at room temperature before flowing into the chambers.

GFP-labeled k560 motors were excited with a 488 nm laser (Sapphire 488–500 CDRH, Coherent), imaged via a custom total internal reflection fluorescence (TIRF) microscope (Nikon 1.49NA, 100× TIRF objective) and recorded using a Photometrics QuantEM 512SC EMCCD camera. Particle tracking and analysis was carried out using a custom-tracking program (Gross Lab) that identifies GFP positions with 2-dimensional Gaussian fitting of their intensity profile.

For single-molecule force measurements using bead assays in the optical trap, sample chambers and motility buffer were prepared as described in the TIRF assays above.

In vitro bead motility assay and force measurements. The truncated kinesin k560 motors and full-length MAP4 used in this study had HIS and FLAG tags at their C-terminus and N-terminus, respectively. For force measurements, the kinesin and MAP4 were specifically linked to the streptavidin-conjugated beads (560 nm diameter, Spherotech) via anti-HIS (biotinylated penta-HIS, Qiagen; and anti-FLAG-biotin) and anti-FLAG (biotinylated, monoclonal anti-FLAG BioM2, F 9291, Sigma-Aldrich) antibodies. The ratio of anti-FLAG to anti-HIS was fixed at 5:1. The incubation of the beads and antibodies was carried out in PEM buffer (80 mM Pipes, 1 mM EGTA, and 4 mM MgSO₄). Briefly, 15 µL anti-HIS (0.2 mg/mL) and 15 µL anti-FLAG (1 mg/mL) were mixed with 50 µL PEM followed by the addition of 10 µL streptavidin beads (1% wt/vol). The mixture was then incubated at 4 °C for 30 min followed by 5 washes in 100 µL PEM buffer supplemented with 4 mg/mL BSA. The beads were stored at 4 °C in the PEM buffer for long-term use of up to 2 wk.

The concentration of MAP4 and MAP4LiCl (*SI Appendix*) during the bead incubations was optimized to approximately 1 µg/mL to minimize the occasional nonspecific binding of beads to the surface and microtubules. Sequential incubation of k560 followed by MAP4 variants was found to work best in finding the kinesin single-molecule activity. The appropriate amount of k560 was added to 30 µL motility buffer followed by the addition of antibody-coated beads and incubation for 6 min at room temperature. Next, MAP4 or MAP4LiCl was added to the above mixture and incubated for a further 6 min at room temperature. The unbound kinesin and MAP4/MAP4LiCl in the solution were removed by pelleting the beads (6,000 *g* for 8 min at 4 °C) and resuspension in 30 µL motility buffer. The mixture was then flown into the sample chamber for single-molecule force measurements using a custom-built optical trapping system capable of detecting forces produced by molecular motors in the pN range.

Data analysis. GraphPad Prism 8.0 software was used for the statistical analyses. Statistical significance was determined using the Student's *t* test ($^{NS}P > 0.05$; $^{*}P < 0.05$; $^{***}P < 0.001$; $^{****}P < 0.0001$).

Data, Materials, and Software Availability. All study data are included in the article and/or *SI Appendix*.

1. N. Hirokawa, Kinesin and dynein superfamily proteins and the mechanism of organelle transport. *Science* 279, 519–526 (1998).
2. R. D. Vale, The molecular motor toolbox for intracellular transport. *Cell* 112, 467–480 (2003).
3. E. Perlson, S. Maday, M. M. Fu, A. J. Moughamian, E. L. Holzbaur, Retrograde axonal transport: Pathways to cell death? *Trends Neurosci.* 33, 335–344 (2010).
4. S. P. Gross, Hither and yon: A review of bi-directional microtubule-based transport. *Phys. Biol.* 1, R1–R11 (2004).
5. W. O. Hancock, Bidirectional cargo transport: Moving beyond tug of war. *Nat. Rev. Mol. Cell Biol.* 15, 615–628 (2014).
6. C. Leidel, R. A. Longoria, F. M. Gutierrez, G. T. Shubeita, Measuring molecular motor forces in vivo: Implications for tug-of-war models of bidirectional transport. *Biophys. J.* 103, 492–500 (2012).
7. M. A. Welte, Bidirectional transport along microtubules. *Curr. Biol.* 14, R525–R537 (2004).
8. M. A. Cianfrocco, M. E. DeSantis, A. E. Leschziner, S. L. Reck-Peterson, Mechanism and regulation of cytoplasmic dynein. *Annu. Rev. Cell Dev. Biol.* 31, 83–108 (2015).
9. N. Hirokawa, Y. Noda, Y. Tanaka, S. Niwa, Kinesin superfamily motor proteins and intracellular transport. *Nat. Rev. Mol. Cell Biol.* 10, 682–696 (2009).
10. K. J. Verhey, J. W. Hammond, Traffic control: Regulation of kinesin motors. *Nat. Rev. Mol. Cell Biol.* 10, 765–777 (2009).
11. C. Conde, A. Cáceres, Microtubule assembly, organization and dynamics in axons and dendrites. *Nat. Rev. Neurosci.* 10, 319–332 (2009).
12. M. K. Mattson-Hoss et al., CK2 activates kinesin via induction of a conformational change. *Proc. Natl. Acad. Sci. U.S.A.* 111, 7000–7005 (2014).
13. R. J. McKenney, M. Vershinin, A. Kunwar, R. B. Vallee, S. P. Gross, LIS1 and NudE induce a persistent dynein force-producing state. *Cell* 141, 304–314 (2010).
14. J. Xu et al., Casein kinase 2 reverses tail-independent inactivation of kinesin-1. *Nat. Commun.* 3, 754 (2012).
15. A. Kunwar et al., Mechanical stochastic tug-of-war models cannot explain bidirectional lipid-droplet transport. *Proc. Natl. Acad. Sci. U.S.A.* 108, 18960–18965 (2011).
16. A. K. Rai, A. Rai, A. J. Ramaiya, R. Jha, R. Mallik, Molecular adaptations allow dynein to generate large collective forces inside cells. *Cell* 152, 172–182 (2013).
17. S. Bodakuntla, A. S. Jijumon, C. Villablanca, C. Gonzalez-Billault, C. Janke, Microtubule-associated proteins: Structuring the cytoskeleton. *Trends Cell Biol.* 29, 804–819 (2019).

18. R. Dixit, J. L. Ross, Y. E. Goldman, E. L. F. Holzbaur, Differential regulation of dynein and kinesin motor proteins by tau. *Science* **319**, 1086–1089 (2008).

19. P. J. Hooikaas *et al.*, MAP7 family proteins regulate kinesin-1 recruitment and activation. *J. Cell Biol.* **218**, 1298–1318 (2019).

20. C. P. Samora *et al.*, MAP4 and CLASP1 operate as a safety mechanism to maintain a stable spindle position in mitosis. *Nat. Cell Biol.* **13**, 1040–1050 (2011).

21. S. R. Tymanskyj, B. H. Yang, K. J. Verhey, L. Ma, MAP7 regulates axon morphogenesis by recruiting kinesin-1 to microtubules and modulating organelle transport. *eLife* **7**, e36374 (2018).

22. M. Vershinin, B. C. Carter, D. S. Razafsky, S. J. King, S. P. Gross, Multiple-motor based transport and its regulation by tau. *Proc. Natl. Acad. Sci. U.S.A.* **104**, 87–92 (2007).

23. M. Vershinin, J. Xu, D. S. Razafsky, S. J. King, S. P. Gross, Tuning microtubule-based transport through filamentous MAPs: The problem of dynein. *Traffic* **9**, 882–892 (2008).

24. C. Ballatore, V. M. Lee, J. Q. Trojanowski, Tau-mediated neurodegeneration in Alzheimer's disease and related disorders. *Nat. Rev. Neurosci.* **8**, 663–672 (2007).

25. Y. Wang, E. Mandelkow, Tau in physiology and pathology. *Nat. Rev. Neurosci.* **17**, 5–21 (2016).

26. A. R. Chaudhary, F. Berger, C. L. Berger, A. G. Hendricks, Tau directs intracellular trafficking by regulating the forces exerted by kinesin and dynein teams. *Traffic* **19**, 111–121 (2018).

27. B. Trinczek, A. Ebneth, E. M. Mandelkow, E. Mandelkow, Tau regulates the attachment/detachment but not the speed of motors in microtubule-dependent transport of single vesicles and organelles. *J. Cell Sci.* **112**, 2355–2367 (1999).

28. J. L. Stern, D. V. Lessard, G. J. Hoeprich, G. A. Morfini, C. L. Berger, Phosphoregulation of tau modulates inhibition of kinesin-1 motility. *Mol. Biol. Cell* **28**, 1079–1087 (2017).

29. N. M. Kanaan *et al.*, Phosphorylation in the amino terminus of tau prevents inhibition of anterograde axonal transport. *Neurobiol. Aging* **33**, 826.e15–826.e30 (2012).

30. G. Lee *et al.*, Phosphorylation of tau by fyn: Implications for Alzheimer's disease. *J. Neurosci.* **24**, 2304–2312 (2004).

31. L. Buée, T. Bussière, V. Buée-Scherrer, A. Delacourte, P. R. Hof, Tau protein isoforms, phosphorylation and role in neurodegenerative disorders. *Brain Res. Brain Res. Rev.* **33**, 95–130 (2000).

32. M. Goedert *et al.*, The abnormal phosphorylation of tau protein at Ser-202 in Alzheimer disease recapitulates phosphorylation during development. *Proc. Natl. Acad. Sci. U.S.A.* **90**, 5066–5070 (1993).

33. J. Avila *et al.*, Tau phosphorylation by GSK3 in different conditions. *Int. J. Alzheimers Dis.* **2012**, 578373 (2012).

34. D. P. Hanger, K. Hughes, J. R. Woodgett, J. P. Brion, B. H. Anderton, Glycogen synthase kinase-3 induces Alzheimer's disease-like phosphorylation of tau: Generation of paired helical filament epitopes and neuronal localisation of the kinase. *Neurosci. Lett.* **147**, 58–62 (1992).

35. D. P. Hanger, A. Seereeram, W. Noble, Mediators of tau phosphorylation in the pathogenesis of Alzheimer's disease. *Expert Rev. Neurother.* **9**, 1647–1666 (2009).

36. D. Hajka *et al.*, GSK3 as a regulator of cytoskeleton architecture: Consequences for health and disease. *Cells* **10**, 2092 (2021).

37. R. Mancinelli *et al.*, Multifaceted roles of GSK-3 in cancer and autophagy-related diseases. *Oxid. Med. Cell. Longev.* **2017**, 4629495 (2017).

38. S. Peineau *et al.*, The role of GSK-3 in synaptic plasticity. *Br. J. Pharmacol.* **153**, S428–S437 (2008).

39. K. Dolma *et al.*, Presenilin influences glycogen synthase kinase-3 β (GSK-3β) for kinesin-1 and dynein function during axonal transport. *Hum. Mol. Genet.* **23**, 1121–1133 (2014).

40. G. Morfini, G. Szebenyi, R. Elluru, N. Ratner, S. T. Brady, Glycogen synthase kinase 3 phosphorylates kinesin light chains and negatively regulates kinesin-based motility. *EMBO J.* **21**, 281–293 (2002).

41. C. Weaver *et al.*, Endogenous GSK-3/shaggy regulates bidirectional axonal transport of the amyloid precursor protein. *Traffic* **14**, 295–308 (2013).

42. F. J. Gao *et al.*, GSK-3β phosphorylation of cytoplasmic dynein reduces Ndel1 binding to intermediate chains and alters dynein motility. *Traffic* **16**, 941–961 (2015).

43. M. Morel, M. Authelet, R. Dedecker, J. P. Brion, Glycogen synthase kinase-3beta and the p25 activator of cyclin dependent kinase 5 increase pausing of mitochondria in neurons. *Neuroscience* **167**, 1044–1056 (2010).

44. J. C. Bulinski, T. E. McGraw, D. Gruber, H. L. Nguyen, M. P. Sheetz, Overexpression of MAP4 inhibits organelle motility and trafficking in vivo. *J. Cell Sci.* **110**, 3055–3064 (1997).

45. I. Semenova *et al.*, Regulation of microtubule-based transport by MAP4. *Mol. Biol. Cell* **25**, 3119–3132 (2014).

46. D. P. McVicker, L. R. Chrin, C. L. Berger, The nucleotide-binding state of microtubules modulates kinesin processivity and the ability of tau to inhibit kinesin-mediated transport. *J. Biol. Chem.* **286**, 42873–42880 (2011).

47. A. Seitz *et al.*, Single-molecule investigation of the interference between kinesin, tau and MAP2c. *EMBO J.* **21**, 4896–4905 (2002).

48. V. Siahaan *et al.*, Kinetically distinct phases of tau on microtubules regulate kinesin motors and severing enzymes. *Nat. Cell Biol.* **21**, 1086–1092 (2019).

49. L. Guillaud, R. Wong, N. Hirokawa, Disruption of KIF17-Mint1 interaction by CaMKII-dependent phosphorylation: A molecular model of kinesin-cargo release. *Nat. Cell Biol.* **10**, 19–29 (2008).

50. K. Tokuraku, T. Q. Noguchi, M. Nishie, H. Matsushima, S. Kotani, An isoform of microtubule-associated protein 4 inhibits kinesin-driven microtubule gliding. *J. Biochem.* **141**, 585–591 (2007).

51. K. Svoboda, S. M. Block, Force and velocity measured for single kinesin molecules. *Cell* **77**, 773–784 (1994).

52. M. C. Caino *et al.*, PI3K therapy reprograms mitochondrial trafficking to fuel tumor cell invasion. *Proc. Natl. Acad. Sci. U.S.A.* **112**, 8638–8643 (2015).

53. J. A. Engelman, J. Luo, L. C. Cantley, The evolution of phosphatidylinositol 3-kinases as regulators of growth and metabolism. *Nat. Rev. Genet.* **7**, 606–619 (2006).

54. B. J. Reddy *et al.*, Load-induced enhancement of dynein force production by LIS1-NudE in vivo and in vitro. *Nat. Commun.* **7**, 12259 (2016).

55. H. Shigematsu *et al.*, Structural insight into microtubule stabilization and kinesin inhibition by tau family MAPs. *J. Cell Biol.* **217**, 4155–4163 (2018).

56. E. Magnani *et al.*, Interaction of tau protein with the dynactin complex. *EMBO J.* **26**, 4546–4554 (2007).

57. B. Cunniff, A. J. McKenzie, N. H. Heintz, A. K. Howe, AMPK activity regulates trafficking of mitochondria to the leading edge during cell migration and matrix invasion. *Mol. Biol. Cell* **27**, 2662–2674 (2016).

58. B. C. Carter, G. T. Shubeita, S. P. Gross, Tracking single particles: A user-friendly quantitative evaluation. *Phys. Biol.* **2**, 60–72 (2005).

The ubiquitous Microtubule Associated Protein 4 (MAP4) controls organelle distribution by regulating the activity of the kinesin motor

Ibtissem Nabti[1], Babu J. N. Reddy[2], Rachid Rezgui[3], Wenqi Wang[2], Steven P. Gross[2], and George T. Shubeita[1*]

Supplementary Information
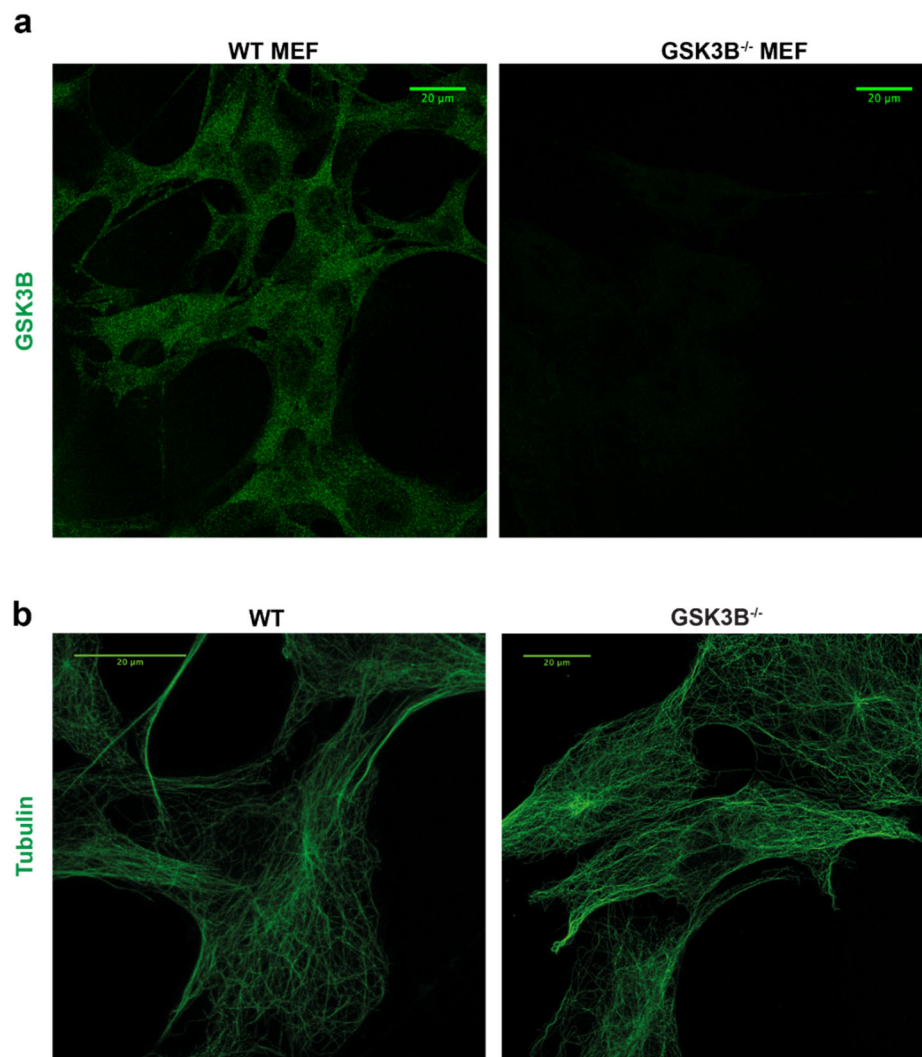
**Supplementary Fig. 1. No traces of GSK3β and intact microtubules in the GSK3β knockout MEFs.** (a) Representative confocal images of WT and GSK3β KO (GSK3B^{-/-}) MEFs immunostained for GSK3β in (a) and microtubules in (b). The images clearly show the absence of any traces of GSK3β and the presence of long intact microtubules in the KO cells. Bars, 20 μm.
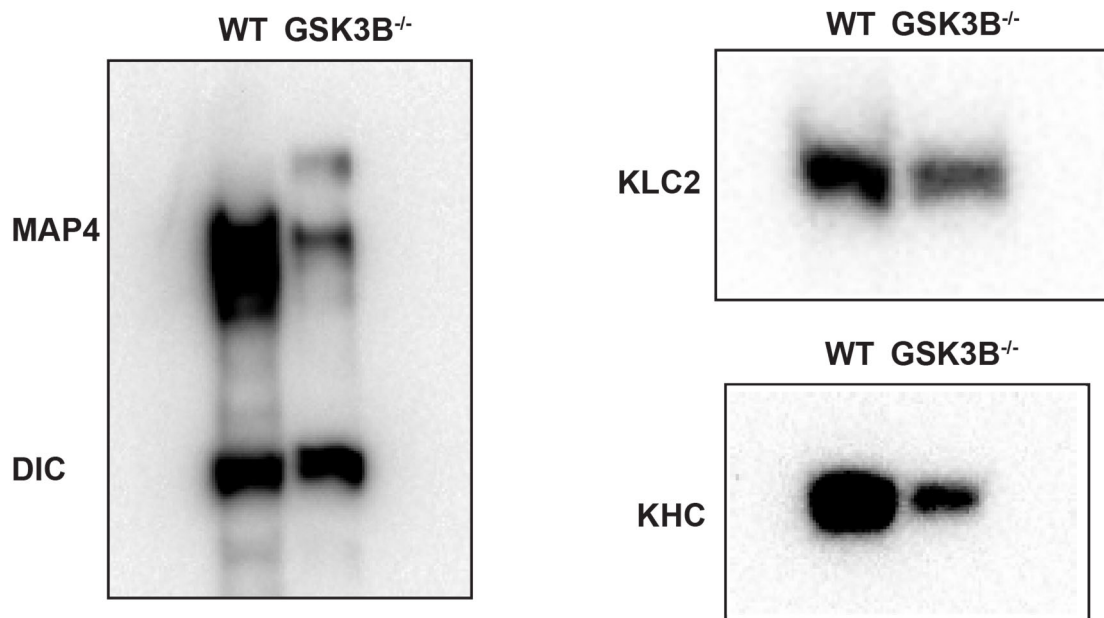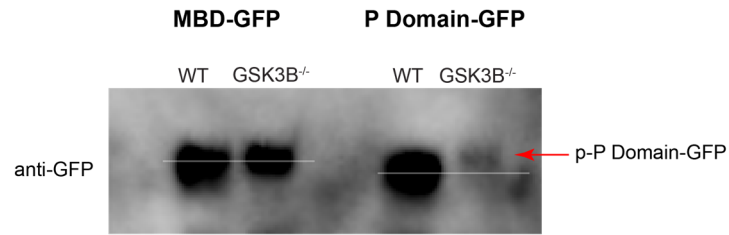
Supplementary Fig. 2. The phosphorylation state of motor subunits is not altered in GSK3β knockout cells. Phosphorylation-affinity electrophoresis coupled with Western blotting of WT and GSK3β KO cell extracts for MAP4, Dynein Intermediate Chains (DIC), Kinesin Heavy Chain (KHC), and Kinesin Light Chain 2 (KLC2) .
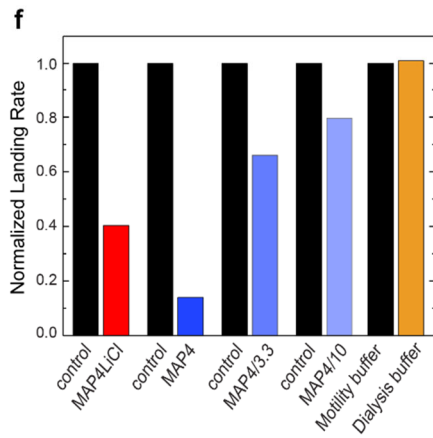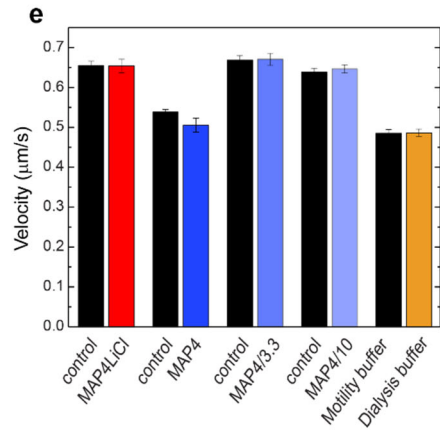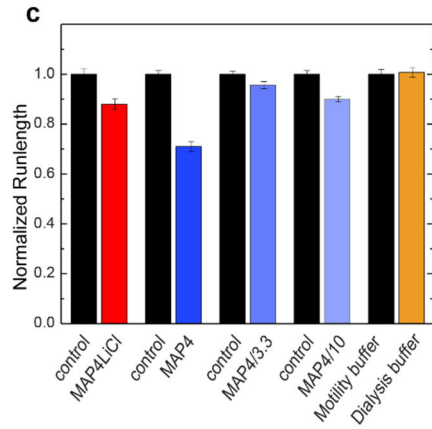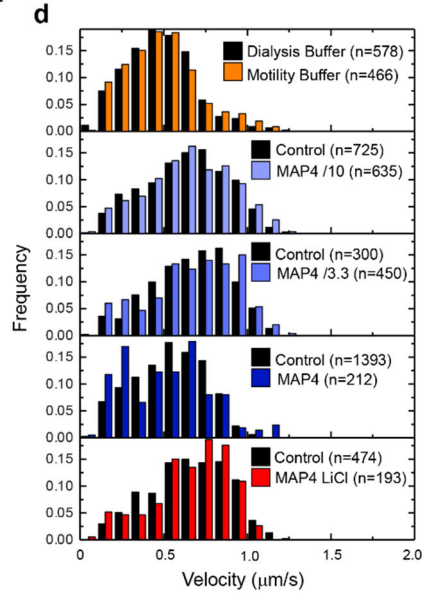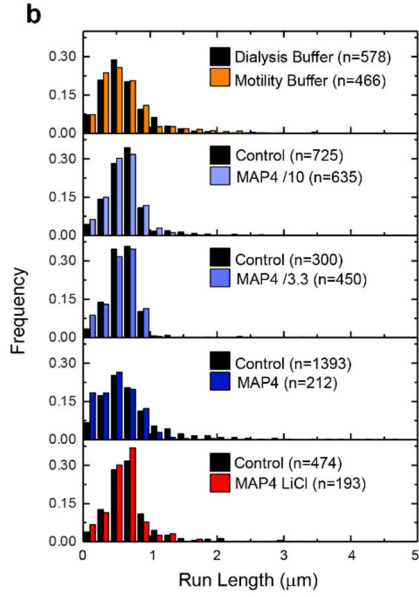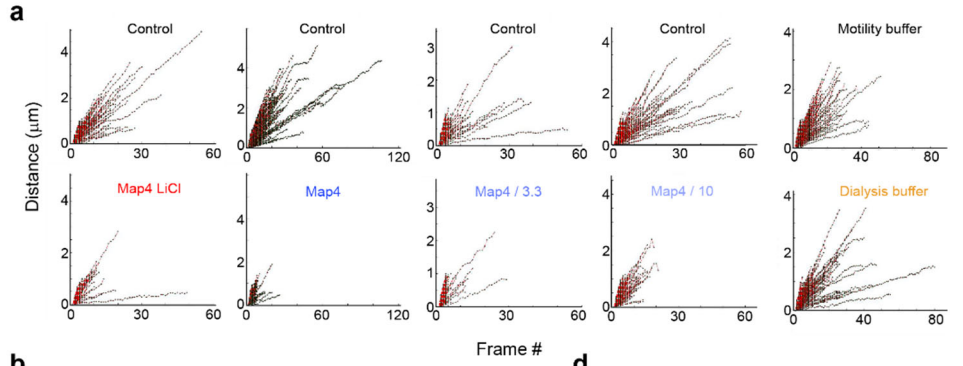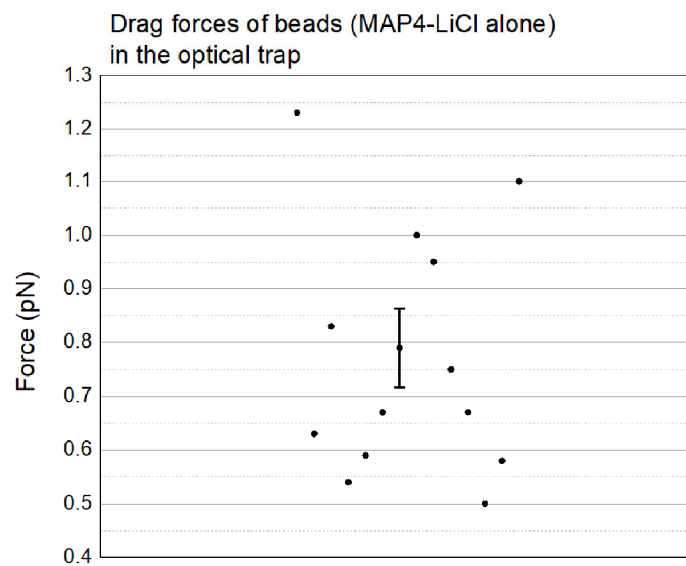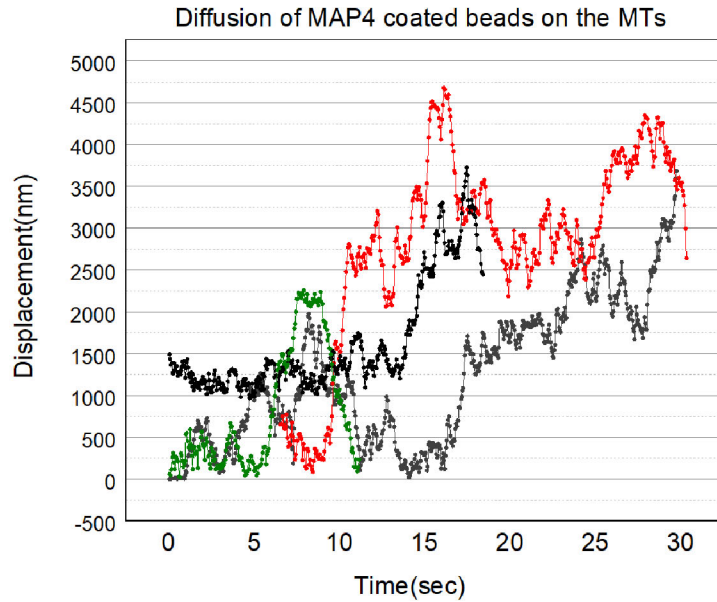
Supplementary Fig. 3. Decorating the microtubules with MAP4 purified from cells where GSK3β was inhibited does not lead to increased kinesin impairment in vitro compared to MAP4 purified from untreated cells. The run length (b,c), velocity (d, e), an landing rate (f) of kinesin (k560) on microtubules is altered in a concentration-dependent manner in the presence of either MAP4 or MAP4 purified from cells where GSK3β was inhibited (MAP4LiCl). The effect of MAP4 from GSK3β-inhibited cells is less pronounced than that of MAP4 from untreated cells at equal concentrations. Sample trajectories are shown in (a), run length and velocity distributions in (b) and (d), and averages in (c) and (e). Experimental samples and their respective controls to which they are compared in the figures above were assayed side-by-side.

Supplementary Fig. 4. The phosphorylation state of the microtubule binding domain (MBD) of MAP4 is not altered in the GDK3β knockout cells. Phosphorylation-affinity electrophoresis coupled with Western blotting of WT and GSK3β KO cell extracts expressing either the GFP-tagged microtubule-binding domain (MBD-GFP) or projection domain (P-domain-GFP). The MBD shows no shift indicating no change in its phosphorylation state in the KO cells. The P-domain expresses poorly in the KO cells, but consistently shows a shift (red arrow) suggesting that it is phosphorylated in the KO cells. The white lines are overlain on the image as a guide to the eye.

Diffusion of MAP4 coated beads on the MTs

Drag forces of beads (MAP4-LiCl alone) in the optical trap

Supplementary Fig. 5. Purified MAP4 attached to beads diffuses along microtubules, and less than 1pN is required to drag the beads along. The top panel shows sample traces showing that polystyrene beads with MAP4 specifically attached to them diffuse along microtubules in vitro in the absence of kinesin. When held using the optical trap and dragged along the microtubule, MAP4-bound beads exert – on average- less than 1pN of opposing force (bottom). The scatter represents multiple measurements on 7 distinct beads with the mean ± SEM indicated.

Supplementary Materials and Methods

Cell culture and Treatments

Wild type (WT) and GSK3β-knockout (GSK3β KO) Mouse embryonic fibroblasts (MEFs), and adenocarcinomic human alveolar basal epithelial cells (A549) (kind gifts from P. Percipalle, New York University Abu Dhabi) were cultured in Dulbecco's modified Eagle's medium (DMEM, D5796, Sigma) or RPMI-1640 (R0883, Sigma) supplemented with 10% fetal bovine serum (F0804, Sigma), penicillin and streptomycin (P4333, Sigma) in a humidified incubator with 5% CO_2 at 37 °C. For GSK3β inhibition, cells were incubated for 24 h in either 40 μM AR-A014418 (A3230, Sigma) or 100 μM SB-415286 (S3567, Sigma). For cytoplasmic dynein inhibition, cells were incubated for 1h in 40 μM Ciliobrevin-D (# 10519074, Millipore).

Cell transfection

MEFs were transiently transfected with the following plasmids: Myc-tagged GSK3β (Tag5Amyc-GSK3b WT, Addgene, plasmid # 16260), mCitrine-tagged C-terminal domain of MAP4 (mCitrine-MAP4-C-10, Addgene, plasmid # 56382), GFP-tagged full MAP4 (Full mouse MAP4 gene cloned by Biosynthesis, then sub-cloned into pcDNA3-EGFP, Addgene, plasmid # 1303) and GFP-tagged MAP4 projection domain (Amplified by PCR using the GFP-tagged full MAP4 vector and the following set of primers: TAAGCAGAATTCCCATGGCCGATCTGAGCCT-forward primer and TGCTTAGCGGCCGCGAACACCGCTACACGGTTC-reverse primer). Transfection was carried out using Lipofectamine 3000 Transfection Kit (L3000-015, Invitrogen), according to the manufacturer's instructions. After transfection, cells were incubated for 24-48 hours for protein expression.

Cells immunofluorescence staining

Cells grown on glass coverslips in 24-well plates were fixed with 4% paraformaldehyde for 15 min and then permeabilized using 0.5% Triton X-100 for 10 min. Permeabilization was followed by 30 min blocking in 1% BSA + 0.1% Tween solution. The cells were incubated overnight with primary antibodies against Alpha-Tubulin (1mg/ml, ab7750, Abcam), MAP4 (1 μg/ml, ab89650, Abcam),

MAP4 (1 µg/ml, A301-489A, Bethyl Laboratories, Inc), c-Myc (10 µg/ml, ab32072, Abcam), KIF5B (1 µg/ml, ab42492, Abcam) and GSK3β (1:250, # 9832, Cell Signaling Technology) at 4 °C. Cells were then washed with PBS buffer, incubated with secondary antibodies (1:250) for 1 h at room temperature and finally mounted onto glass slides with mounting media (Vectashield, LSBio). The cells were subsequently imaged using Leica TCS SP8 X Fluorescence Microscope (Leica, Germany) and acquired images analyzed using ImageJ software.

Lipid droplets purification

Ten 10-cm dishes of WT and GSK3β KO MEFs, pre-incubated overnight in 1mg/ml Oleic acid, were washed twice with cold PBS and re-suspended in 500 µl of homogenization buffer (50 mmol/liter Tris-HCl, pH 7.5, 150 mmol/ liter sodium chloride, and 5 mmol/ liter EDTA), supplemented with 10 µg/ml leupeptin and 10 µg/ml aprotinin. Cells were disrupted at 4°C by nitrogen cavitation in a cell disruption bomb (# 4639; Parr Instrument Company) at 800 psi for 15 min and collected dropwise. Afterward, cells were passed back and forth through a 21-gauge needle 10 times at 4°C. Nuclei and unbroken cells were removed by centrifugation at 1,800 g for 5 min at 4°C. The resulting supernatant was mixed with 2.4M sucrose to a final concentration of 1.4M and loaded at the bottom of a discontinuous sucrose gradient formed by layers of 1.1, 0.8, 0.6 and 0.3M sucrose freshly prepared in homogenization buffer. Gradients were centrifuged in a 90 Ti fixed-angle rotor (Optima XPN-90 Ultracentrifuge, Beckman Coulter) without brake at 35,000 rpm for 1.5 h at 4°C. Lipid droplets that reached the top layer were collected by gently scarping the sides of the centrifuge tube, mixed 10 times by pipetting and snap frozen in liquid nitrogen prior to storage at -80°C.

Lipid droplets immunofluorescence staining

Purified lipid droplets were embedded in Matrigel Matrix (# 2055463, Corning, Arizona) supplemented with 0.2M Na_3PO_4 and 0.1M NaOH. The Matrigel/lipid droplets mix was then spread on a pre-cleaned glass coverslip and incubated at 37°C for 30 min. This was followed by fixation in 4% paraformaldehyde for 45 min, washing with PBS and blocking in 1% BSA + 0.1% Tween solution for 30 min. The coverslips were incubated overnight with primary antibodies

against MAP4 (1 μg/ml, ab89650, Abcam), KIF5B (1 μg/ml, ab42492, Abcam) and Dynein-intermediate chains 1/2 (2 μg/ml, sc-13524, Santa Cruz, Biotechnology) at 4 °C. Coverslips were then washed with PBS buffer, incubated with secondary antibodies (1:250) for 1 h at room temperature, stained with 1 μg/ml Nile Red (N1142, Thermo Fisher Scientific) for 30 min and finally mounted onto glass slides with mounting media (Vectashield). Finally, the lipid droplets were imaged using Leica TCS SP8 X Fluorescence Microscope (Leica, Germany) and acquired images analyzed using ImageJ software.

Immunoprecipitation

Immunoprecipitation was carried out using the Thermo Scientific Pierce Classic IP Kit (# 26146) according to the manufacturer's instructions. Briefly, WT and GSK3β KO MEFs were lysed using the IP lysis buffer provided with the kit and centrifuged for 10 min at 4°C. Following centrifugation, the concentration of the proteins in the supernatant was measured using Thermo Scientific Pierce BCA Protein Assay Kit (# 23225). 1.2 mg of protein lysate was mixed with 5μg of anti-MAP4 (ab89650, Abcam), or rabbit IgG (I5006, Sigma) antibodies and incubated overnight at 4 °C under agitation. Protein A/G coupled Agarose beads were then used to pull down the antibody/antigen complex from the samples. Finally, the antibody/antigen complex was eluted using 2X Non-reducing sample buffer supplemented with 20Mm DTT, boiled for 10 minutes at 100°C and used for Western blotting. Otherwise, the immune complex was recovered via incubation for 10 min in the provided low-pH elution buffer, which was then neutralized using 1M Tris, pH 9.5 and sent for mass-spectrometry analysis (Fingerprints Proteomics Facility, Dundee, UK).

Western blotting

Samples were fractionated at 200V for 1hr 30min on a Mini Protean Tetra Cell (Bio-Rad, UK) using 8% SDS PAGE gels or SuperSep™ Phos-tag™ pre-cast gels (# 198-17982, Wako, Japan) for the phosphorylation-affinity electrophoresis. Proteins were blotted onto polyvinylidene fluoride membranes (PVDF) for 1h 30min at 100V. Anti-MAP4 (1:1000, sc-390286, Santa Cruz Biotechnology), anti-DIC1/2 (1:500), anti-Kinesin 1 (1:500, AKIN01, Cytoskeleton) and anti-ADFP

(1:500, ab108323, Abcam) were used for Western blotting. Protein bands were detected using the ChemiDoc MP Imaging system (Bio-Rad).

MAP4 purification

Human MAP4 Isoform2, expressed in HEK293 cells, was purified from untreated cells (MAP4) and cells incubated overnight in 25mM LiCl (MAP4LiCl) to inhibit GSK3 phosphorylation, with increased beta-catenin levels used to confirm GSK3 inhibition. Purified MAP4 was eluted in NETN lysis buffer with biotin. This buffer affected kinesin motility in control experiments. Hence, to reduce the effect of this buffer on kinesin motility, dialysis was carried out for 2 hours at 4°C using Slide-A-Lyzer Mini Dialysis units (#69576, Thermo Scientific) according to the manufacturer's instructions. Motility Assay Buffer without ATP or GTP was used as exchange buffer during dialysis.

Analysis of cargo distribution

Distribution of MitoTracker-labeled mitochondria and Nile red-labeled lipid droplets (fig. 2, 4, 7) was analyzed using ImageJ. The distribution was represented as percentage of whole cell surface area and was calculated according to the formula (ROI^M/ROI^C*100), where ROI^M and ROI^C represent Regions of Interests manually drawn around the distributed organelles and whole cell, respectively.
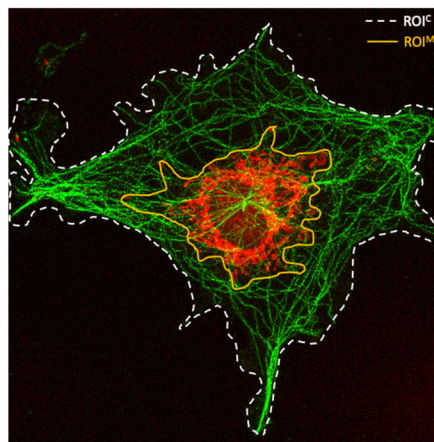
Example of cargo distribution analysis. Cargo distribution was calculated as ROI^M/ROI^C*100 , where ROI^M (Yellow dashed line drawn around the distributed cargo) and ROI^C (White dashed line drawn around whole cell).